Nanotube Structures

DOI: 10.1002/anie.201104520

Synthesis of Copious Amounts of SnS_2 and SnS_2/SnS Nanotubes with Ordered Superstructures**

*Gal Radovsky, Ronit Popovitz-Biro, Matthias Staiger, Konstantin Gartsman, Christian Thomsen, Tommy Lorenz, Gotthard Seifert, and Reshef Tenne**

Nanoparticles of layered (two-dimensional, 2D) compounds are known to be unstable in the planar form, forming instead closed polyhedral inorganic fullerene-like (IF) nanoparticles and also inorganic nanotubes (INT). Their formation was attributed to the annihilation of the dangling bonds of the rim atoms. IF nanoparticles either of SnS_2 or having a SnS_2–SnS ordered superstructure and short tubules thereof were reported in the past.[1,2] Very recently, SnS_2 INTs were synthesized by the vapor–liquid–solid (VLS) technique utilizing bismuth as a liquid catalyst.[3] INTs of misfit-layered compounds[4] have been known for a long time.[5] In analogy to chrysotile (asbestos) nanotubes,[6] the driving force for the formation of nanotubes of misfit compounds stems from the asymmetry along the c axis of the unit cell.[5]

The phase diagram of the Sn–S system[7] shows three main compounds: tin monosulfide SnS, Sn_2S_3, and tin disulfide SnS_2. α-SnS (herzenbergite) has a GeS structure with an orthorhombic (pseudo-tetragonal highly distorted NaCl) unit cell ($a = 1.118$, $b = 0.398$, $c = 0.432$ nm; $Pnma$).[8] α-SnS_2 has a CdI_2 layered (trigonal-1T) structure with a pseudo-hexagonal unit cell ($a = 0.36486$ and $c = 0.58992$ nm).[2,9] The Sn–S system can be regarded as a misfit-layered compound and the tubular morphology[2,5] is a result of the lattice mismatch between the two alternating layers of SnS_2 and SnS sublattices, which leads to intrinsic stress in the SnS_2/SnS superstructure sheets. This driving force comes in addition to the already established closure mechanism, that is, annihilation of dangling bonds at the periphery of the layers of the INT nanostructures. The combination of these driving forces leads to the formation of nanoscrolls and nanotube morphologies as shown in Figure 1. The Sn–S system was used in the past to demonstrate a solar battery, that is, a solar cell in parallel with a Sn–S electrode which delivers constant power day and night.[10]

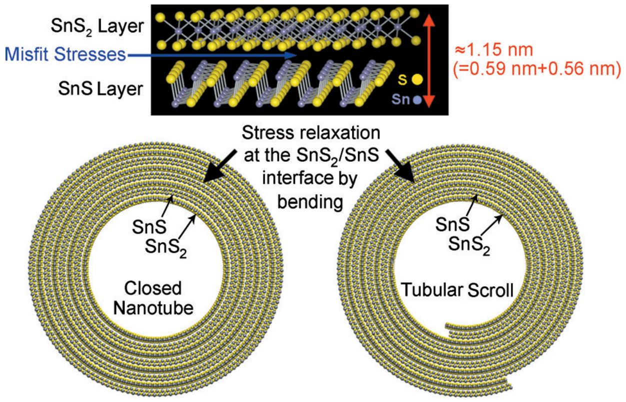

Figure 1. Depiction of the tubular structures of the SnS_2/SnS ordered superstructure. Pseudo-hexagonal trigonal (T) SnS_2 and orthorhombic (O) SnS layers with interlayer spacings of 0.59 nm and 0.56 nm, respectively, relax misfit stress by forming tubular scrolls and closed nanotubes.

The alternate stacking of MX and TX_2 (M = Sn, Pb, Sb, Bi, and rare-earth metals; T = Sn, Ti, V, Cr, Nb, Ta; X = S, Se) in misfit-layered compounds is thought to be stabilized also by a partial charge transfer (CT) from the MX layer to the TX_2 layer. Therefore, the larger the CT, the stronger the interaction between the layers, and the (more rigid) the superstructure (increased 3D character).[11]

The tubular structures reported herein were analyzed by transmission electron microscopy (TEM) and high-resolution TEM (HRTEM) and can be classified into three main groups: 1) SnS_2/SnS ordered-superstructure nanoscrolls and 2) nanotubes, and 3) pure SnS_2 nanotubes. Their diameters range from 13–165 nm and their lengths from 90 nm to 3.2 μm. The number of layers varies from 3–40. Bending of the nanosheets produces nanotubes or nanoscrolls with several possible stacking orders. The scrolling process characterized by scanning electron microscopy (SEM) of a few SnS_2/SnS molecular-layer sheets is shown in Figure 2a and marked by red arrows in Figure 2b. The gradual conversion of micrometric SnS_2 platelets into nanotubules through the catalytic action of Bi

---

[*] G. Radovsky, Dr. R. Popovitz-Biro, Dr. K. Gartsman, Prof. Dr. R. Tenne
Department of Materials and Interfaces
Weizmann Institute of Science
Rehovot 76100 (Israel)
E-mail: Reshef.Tenne@weizmann.ac.il
Homepage: http://www.weizmann.ac.il/materials/tenne

M. Staiger, Prof. C. Thomsen
Institut für Festkörperphysik, Technische Universität
Hardenbergstrasse 36, 10623 Berlin (Germany)

T. Lorenz, Prof. G. Seifert
Physikalische Chemie, Technische Universität Dresden
Bergstrasse 66b, 01062 Dresden (Germany)

[**] We thank Dr. A. N. Enyashin for preparing the atomistic model, Dr. P. von Huth for expert FIB assistance, and Dr. L. Houben and Dr. V. Lyakhovitskaya for useful discussions. R.T. gratefully acknowledges the support of ERC (project INTIF 226639), the Israel Science Foundation, (c) the Harold Perlman Foundation, The GMJ Schmidt Minerva Center, and the Irving and Cherna Moskowitz Center for Nano and Bio-Nano Imaging. R.T. is the Drake Family Chair in Nanotechnology and director of the Helen and Martin Kimmel Center for Nanoscale Science.

Supporting information for this article is available on the WWW under http://dx.doi.org/10.1002/anie.201104520.

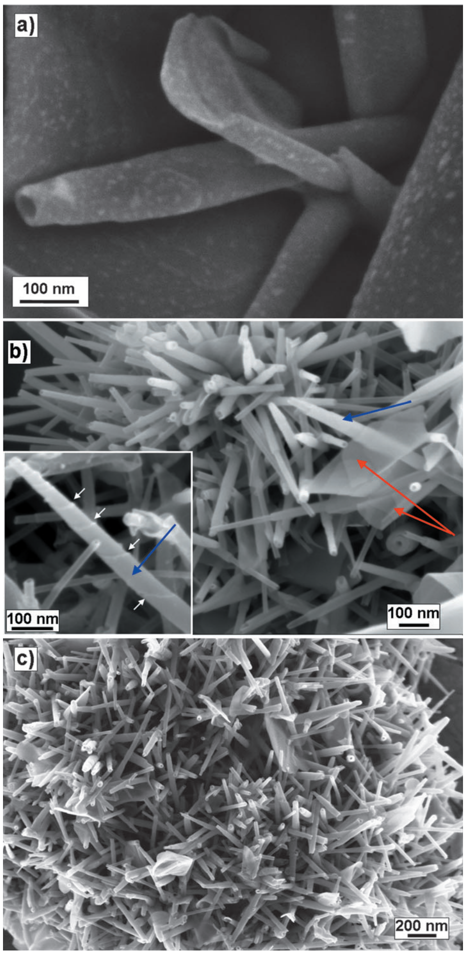

Figure 2. a) High magnification backscattering electrons (BSE) SEM image illustrating the exfoliation/scrolling of SnS_2/SnS misfit layers into tubular (scroll) structures. Sulfides of bismuth appear as bright spots in the BSE contrast. b) Secondary electrons (SE) image of tubule's agglomerate. Red arrows indicate nanosheets in the midst of a scrolling process. Blue arrows point to nanoscrolls exhibiting helical wound growth step which can be clearly seen in the inset and is marked by short white arrows. c) SE image of macroscopic amounts of nanotubes, nanoscrolls and several unscrolled nanosheets.

and Sb_2S_3 is demonstrated in Figures S1 and S2 in the Supporting Information. By the end of the process the platelets are completely converted into either nanotubes, nanoscrolls, or unscrolled nanosheets as can be seen in Figure 2c and Figure S2d in the Supporting Information.

Energy-dispersive X-ray spectroscopy (EDS) analysis of individual nanotubes (see also Figure S3 in the Supporting Information) shows that the S/Sn ratio varies between 1.2:1 and 1.4:1,[2] suggesting the existence of superstructures. Furthermore, the bismuth concentration (5 atom %) was found to be uniform along the nanotube axis. The tubules including the bismuth remained stable under the electron beam of 120 kV. These facts suggest that the bismuth forms a high-melting sulfide, residing either inside the core of the tubes or trapped between the layers. The antimony profile was also constant along the tube axis (0.5–2 atom %), when added to the reaction mixture. A representative X-ray diffraction (XRD) pattern of the whole product is shown in Figure S4 in the Supporting Information.

Since Bi has a relatively high vapor pressure (1.03×10^{-4} atm at 793 °C[12]), it evaporates and reacts with sulfur vapor. Bi_2S_3 deposits as small spots on the platelet surface, which can be easily resolved by scanning transmission electron microscopy (STEM) utilizing a high-angle annular dark-field (HAADF) detector and also by the signal of back-scattered electrons (BSE) in SEM (see Figure 2a and also Figure S2a,b in the Supporting Information). This surface reaction causes a partial decomposition of the trigonal (T) SnS_2 precursor to a more sulfur-deficient structure, that is, to orthorhombic (O) SnS. These two layers form a misfit-layered compound of the type $(SnS)_n(SnS_2)_m$ (see Section 1.2 in the Supporting Information for an illustration). The lattice mismatch between the two layers creates internal stress which causes the layers to exfoliate and scroll. The scrolling process was promoted by the addition of miniscule amounts of Sb_2S_3 powder to the ampoules. The affinity of antimony (which is also a substitutional donor) to sulfur is also very high. However, no Sn–S tubular structures were observed in the absence of Bi. Thus, the added Sb_2S_3 seems to act as a co-catalyst promoting the growth of the Sn–S nanotubes. Adding SnS to SnS_2 in small amounts increased the production yield of the ordered-superstructure nanotubes. Apparently, temperature gradients are essential for the growth of the Sn–S tubules. The optimum yield was obtained when the colder edge was kept at approximately 250 °C.

Pure SnS_2 nanotubes like that shown in Figure 3a were rarely encountered in this series of experiments (for more details see Section 1.6 in the Supporting Information). The tube consists of evenly spaced fringes which correspond to the interlayer spacing of 0.59 nm of the {00.1} planes along the *c* axis. This spacing is typical of a bulk 1T single crystal of SnS_2.[9] The corresponding spots with higher orders *00.n* are marked by white arrows on the diffraction pattern in Figure 3a. The tubule axis is marked by a purple double arrow. The spots pertinent to the Miller indices *10.0*, *10.1*, *11.0* are marked by dotted rings on the diffraction pattern and correspond to interplanar distances of 3.17, 2.75, and 1.83 Å respectively.[9] All the shells in this tube seem to be helical with a similar chiral angle ($\approx 4°$) which can be estimated from the splitting of the *10.0* reflections at the diffraction pattern in Figure 3a.

In the majority of cases, an ordered superstructure with an asymmetric layer stacking of (orthorhombic, O) SnS, and (trigonal, T) SnS_2 in the order O-T, O-T… could be observed according to the lattice spacing of 1.15 nm, or O-T-T, O-T-T… with a lattice periodicity of roughly 1.74 nm along the *c* axis. Figure 3b shows an example of a commonly encountered cylindrical scroll exhibiting a helically wound growth step.[5] The *c*-axis periodicity of the structure is 1.74 (0.56 + 0.59 + 0.59) nm which corresponds to the O-T-T… ordered superstructure. The diffraction pattern clearly shows a series of equidistant, closely spaced arrays of spots parallel to the two "*c*" directions which pass through other {*hkl*} diffraction spots. These equidistant spots of different orders *00n* (marked by blue arrows) correspond to a superstructure periodicity of 1.74 nm. The spots with Miller indices of *00.1, 10.0*, *11.0* (in

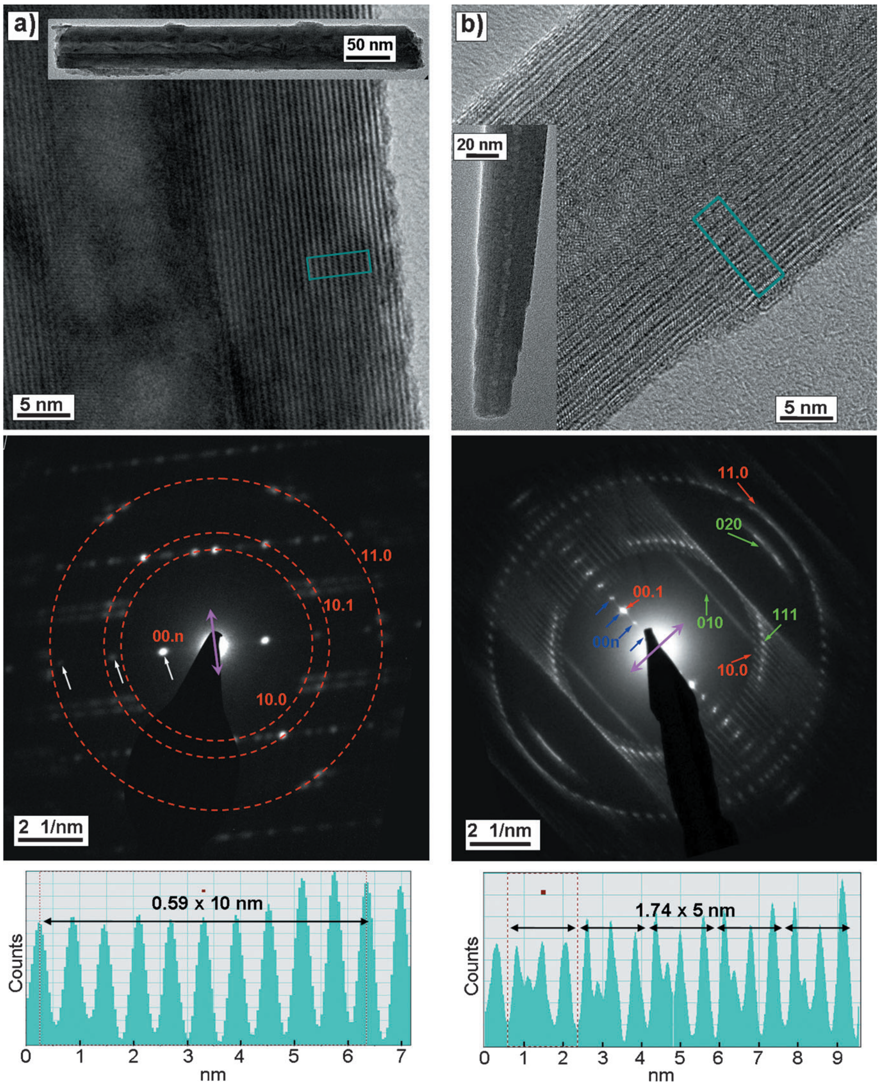

Figure 3. a) TEM image of a pure SnS_2 nanotube. Top: High-resolution TEM (HRTEM) image and at low resolution in the inset. Middle: Selected area electron diffraction (SAED) pattern taken from the area marked in the high-magnification image. Tubule axis is marked by a purple double arrow and coincides with the HRTEM image. Bottom: Line profile integrated along the region marked in the upper image. b) A SnS_2 (T)/SnS (O) ordered-superstructure cylindrical nanoscroll exhibiting a helically wound growth step. Top: High-resolution image and at low resolution in the inset. Middle: SAED pattern taken from the area marked in the high-magnification image. Red, green, and blue arrows indicate diffraction spots obtained from pristine SnS_2 (T), pristine SnS (O), and the T-T-O... ordered superstructure, respectively. The tubule axis is marked by a purple double arrow and coincides with the HRTEM image. Bottom: Line profile integrated along the region marked in the upper image.

hexagonal systems *hk.l* is equivalent to the notation *hkil* with $i=-(h+k)$) marked on the diffraction pattern in Figure 3b with red arrows are attributed to SnS_2 and correspond to interplanar distances of 5.9, 3.06, and 1.75 Å, respectively. The spots with Miller indices of *010*, *111*, *020* marked with green arrows are attributed to SnS and correspond to interplanar distances of 3.99, 2.84, and 1.99 Å, respectively, which are in good agreement with the values of 3.98, 2.83, and 1.99 Å of bulk SnS.[8] It is believed that the streaks on the *10.0* reflection spots arise from the wound stepped growth with varying scrolling angle along the tubule axis, as can be clearly seen in the inset of Figure 3b. The multiple splitting of the *10.0* spots into a ring-like pattern indicates the presence of multiple helicities. A typical SEM image of such scrolls is also shown in the inset of Figure 2b. In addition to nanoscrolls, superlatice nanotubes are also commonly encountered, examples of which are shown in Figure S5 in the Supporting Information.

As a first attempt to understand the observed tubular structures, we performed quantum mechanical calculations (DFTB) of individual SnS_2 and SnS nanotubes. The calculated strain energy E_{str} for individual SnS and SnS_2 nanotubes as a function of tube radius (R) is shown in Figure 4 and follows roughly the relation $E_{str}=\alpha/R^2$. The strain factor α indicates the magnitude of the curvature of the E_{str}–R curves. The values of α were calculated from the strain energy curves of MoS_2 INTs, SnS (n,0) zigzag, SnS (n,n) armchair, SnS (0,n) zigzag, SnS_2 (n,0), SnS_2 (n,n) INTs, and carbon nanotubes (CNTs) and were found to be 27.2, 21.67, 10.78, 5.3, 5.65, 5.29, 2.2 eV Å^2 per atom, respectively. The strain energy of all types of SnS and SnS_2 nanotubes and nanoscrolls is larger than that of CNT and smaller than that of MoS_2 (WS_2) nanotubes.

Similarly to CNT and MoS_2 INTs, the strain energy of INT-SnS_2 is nearly chirality independent. However, in the case of SnS INTs, the elastic energy is critically dependent on the folding vector. This dependence is not surprising in view of the large asymmetry along the two in-plane axes of the nanotubes (see insets in Figure 4). The elastic energy required to bend an SnS layer in the (n,0) zigzag direction is appreciably higher than that required for the (0,n) direction. Therefore, (0,n) SnS nanotubes should be lower in energy than SnS nanotubes with other roll-up vectors, and should exhibit the lowest strain energy for a specific diameter. Not surprisingly, therefore, the diffraction pattern of the SnS_2/SnS ordered-superstructure nanotube in Figure 3b shows that the [010] direction of SnS coincides with the tubule axis. Since the tubule's axis and the roll-up vector are orthogonal, the roll-up vector is dictated to be [00n], forming (0,n) zigzag SnS nanotubes in full agreement with the theoretical predictions.

The nanotube synthesis was scaled up to 10–20 mg quantities in a flow reactor. The synthesis was first accomplished in a horizontal reactor and later on in the vertical

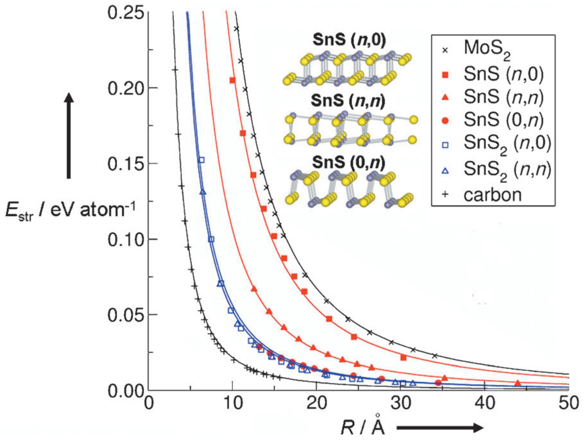

Figure 4. Calculated strain energy E_{str} as a function of the tube radius R for SnS_2 and SnS nanotubes. Values for MoS_2 INTs and carbon nanotubes (CNT) are shown for comparison. The inset shows SnS layers from the two (0,n), (n,0) zigzag, and (n,n) armchair directions. The yellow and violet circles represent sulfur and tin atoms, respectively.

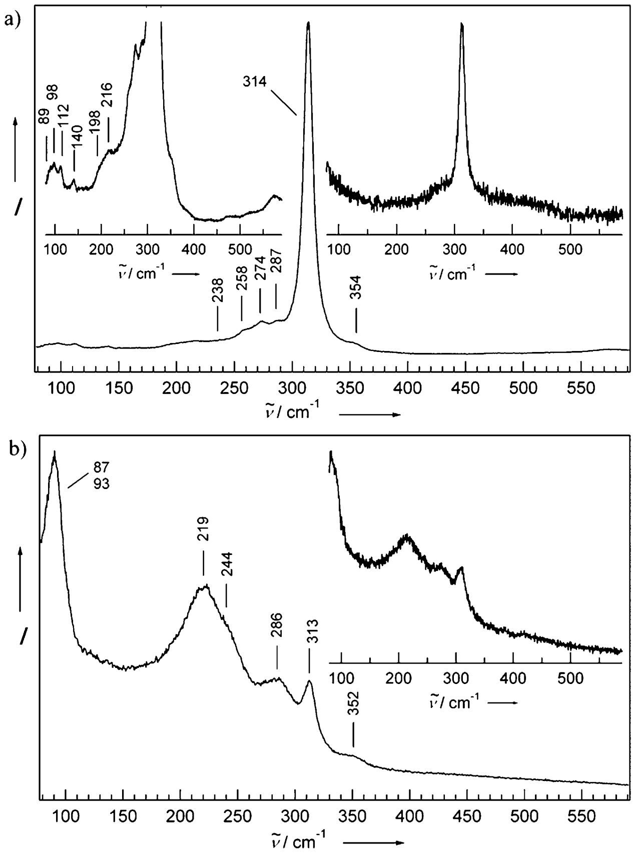

Figure 5. Raman spectra of individual SnS_2 and SnS_2/SnS ordered-superstructure nanotubes (laser wavelength: 532.252 nm). a) Main plot and left inset: Raman spectrum of a SnS_2 nanotube (diameter $d=152$ nm; analyzed by SEM). Right inset: Raman spectrum of a SnS_2 nanotube ($d=91$ nm; TEM). b) Main plot: Raman spectrum of a SnS/SnS_2 ordered-superstructure nanotube ($d=57$ nm; SEM). Inset: SnS/SnS_2 ordered-superstructure nanotube ($d=75$ nm; TEM). A Lorentzian lineshape curve-fitting analysis was done to determine the position of the Raman modes.

configuration shown in Figures S7 and S8 in the Supporting Information. In both cases the tubes were obtained in high yields (>50%). They were much thinner (13–47 nm) and shorter (90–300 nm) than those obtained in the closed ampoules. Also, the tubes were straight and no nanoscrolls were observed in the product of the flow reactors. It is believed that the main growth mechanism in this case is the VLS process with Bi serving as the sole catalyst (see Section 2 in the Supporting Information for a detailed description).

Raman measurements were carried out on well-characterized (either SEM or TEM) individual SnS_2 and SnS_2/SnS ordered-superstructure nanotubes and powders thereof. For this purpose the individual nanotubes were deposited on well-defined locations of SEM stubs and TEM grids (see the Supporting Information for details). Figure 5 shows Raman spectra of individual nanotubes representative of two types of structures, that is, almost pure SnS_2 nanotubes and SnS/SnS_2 ordered-superstructure nanoscrolls/nanotubes. The observed Raman modes can be attributed to either SnS_2 or SnS, with frequencies close to those found in Raman spectra of their respective bulk counterparts.

Dominating the Raman spectrum in Figure 5a is the peak at 314 cm^{-1}, which can be assigned to the A_{1g} mode of SnS_2.[13,14] A closer look (left inset) at the spectrum reveals second-order Raman bands of SnS_2 (140 cm^{-1} and features above 450 cm^{-1}) as well as the appearance of an IR-active A_{2u} mode at around 354 cm^{-1}, which is frequently observed also in Raman spectra of SnS_2 materials.[14,15] The right inset shows the Raman spectrum of another SnS_2 tube analyzed by TEM. To prevent failure of the carbon film, the laser intensity was reduced and hence the spectrum has a lower signal-to-noise ratio. Additionally, first-order Raman modes of SnS occur with comparably weak intensity at 89, 98, 112, 198, 216, 274, and 287 cm^{-1},[16,17] as identified by a Lorentzian lineshape-fitting procedure. They may arise from a few SnS/SnS_2 ordered-superstructure layers closest to the core (as shown in Figure S5b in the Supporting Information). Traces of Bi_2S_3 might also be present as indicated by the small shoulders around 238 and 258 cm^{-1}.[18]

Shown in Figure 5b is a Raman spectrum typical for misfit layer SnS/SnS_2 nanotubes/nanoscrolls (SEM analyzed). The inset shows the Raman spectrum of a similar TEM-analyzed nanotube. Here again the excitation intensity was reduced to prevent failure of the carbon-coated Cu TEM grid. The peaks at 87 and 286 cm^{-1} are attributed to B_{2g} modes of SnS, while the modes at 93 cm^{-1} and the broad feature centered at about 219 cm^{-1} belong to SnS A_g modes[16] with an unidentified shoulder at 244 cm^{-1}. The peaks at 313 and 352 cm^{-1} are assigned to the A_{1g} and A_{2u} modes which serve as a fingerprint for SnS_2. The observation that they appear at almost the same position as in the Raman spectra of the pure SnS_2 nanotubes is indicative of weak SnS_2-SnS coupling. Small shifts of SnS_2 and SnS modes with respect to signals of bulk materials may originate from charge transfer from the SnS layer to the SnS_2 layer and to misfit strain.

In conclusion, the present work reports the synthesis and characterization of SnS_2 and SnS_2/SnS ordered-superstructure nanotubes. The growth of ordered-superstructure nanotubes and nanoscrolls was promoted by the relaxation of misfit stress between the adjacent SnS_2 and SnS layers. Partial decomposition of the SnS_2 precursor to a more sulfur-deficient SnS was stimulated by Bi and Sb_2S_3, which was manifested in the exfoliation of layers and scrolling. The yield of the nanotube synthesis was drastically enhanced by the addition of minute amounts of Sb_2S_3. Constant Bi and Sb profiles were observed along the tubules. Pure SnS_2 nanotubes were also formed, probably as a result of the annealing of preformed ordered-superstructure nanotubes. The presence of the two main structures was confirmed by HRTEM and Raman spectroscopy. Quantum mechanical calculations of the elastic energy of the SnS_2 and SnS nanotubes were carried out as a function of their diameter and chirality. It was shown that the structure of the ordered-superstructure nanotube is dictated by the low folding energy of the zigzag SnS $(0,n)$ tube, which was indicated by electron diffraction analysis. Successful scaling up of the syntheses of SnS_2/SnS ordered-superstructure and pure SnS_2 tubes was accomplished with horizontal and subsequently vertical flow reactors. Possible applications for the present nanotubules can range from batteries[10] and photocatalysts[19] to toxic gas sensors.[20]

Experimental Section

Quartz ampoules were filled with SnS_2 (Alpha Aesar 99.5 %) and Bi (Fluka 99.999 %) powders (5:1 molar ratio). Minuscule amounts of Sb_2S_3 (Cerac/Pure 99.999 %) powder was also used in several experiments. The ampoules were sealed in a vacuum of 2×10^{-5} torr and inserted into a horizontal two-zone reactor furnace. The performed high-temperature annealing procedure involved two main steps: First the whole ampoule was heated to 780 °C for 2 h. Next, it was subjected to a temperature gradient of 780–250 °C for 1.5 h, and was then cooled to room temperature. The product accumulated in the cold zone of the ampoule. Carbon/collodion-coated Cu TEM grids and SEM stubs based on Si/Al substrates were prepared by dripping several droplets from the product solution.

The resulting samples were examined by transmission electron microscopy (TEM; Philips CM120 operating at 120 kV, equipped with an energy-dispersive X-ray spectroscopy (EDS) detector (EDAX-Phoenix Microanalyzer) for chemical analysis), and by high-resolution TEM (FEI Technai F30-UT, with a field-emission gun operating at 300 kV). Scanning transmission electron microscopy (STEM; FEI Tecnai F20 operating at 200 kV equipped with high-angle annular dark field (HAADF) detector and (EDS) detector (EDAX-Phoenix Microanalyzer)), and also scanning electron microscopy (SEM; Zeiss Ultra model V55 and LEO model Supra 55VP equipped with EDS detector (Oxford model INCA) and backscattering electron (BSE) detector) were utilized. For Raman spectroscopy, a frequency-doubled Nd:YAG laser emitting $\lambda = 532.252$ nm light and a LabRAM HR 800 spectrometer (HORIBA, Jobin Yvon) with a 1800 mm grating and a spectral resolution of about 1 cm^{-1} were used. Individual nanotubes were placed on Si wafers (for SEM analysis) and also on carbon- and Si_3N_4-membrane-coated TEM grids (see the Supporting Information for the sample preparation).

The density-functional-based tight-binding method (DFTB) with periodic boundary conditions[21,22] was used for the quantum chemical calculations. In this approximation the LCAO ansatz (linear combination of atomic orbitals) is used for the molecular orbitals and a minimal set of atomic valence orbitals obtained from self-consistent density functional theory (DFT) calculations of the isolated atoms is taken as a basis. The repulsion is described by parameterized short-range two-body potentials.

Received: June 30, 2011

Keywords: chalcogenides · nanotubes · ordered superstructures · tin

[1] B. Alperson M. Homyonfer, R. Tenne, *J. Electroanal. Chem.* **1999**, *473*, 186 – 191.
[2] S. Y. Hong, R. Popovitz-Biro, Y. Prior, R. Tenne, *J. Am. Chem. Soc.* **2003**, *125*, 10470 – 10474.
[3] A. Yella, E. Mugnaioli, M. Panthofer, H. A. Therese, U. Kolb, W. Tremel, *Angew. Chem.* **2009**, *121*, 6546 – 6551; *Angew. Chem. Int. Ed.* **2009**, *48*, 6426 – 6430.
[4] J. Rouxel, A. Meerschaut, G. A. Wiegers, *J. Alloys Compd.* **1995**, *229*, 144 – 157.
[5] D. Bernaerts, S. Amelinckx, G. Van Tendeloo, J. van Landuyt, *J. Cryst. Growth* **1997**, *172*, 433 – 439.
[6] G. Falini, E. Foresti, M. Gazzano, A. F. Gultieri, M. Leoni, I. G. Lesci, N. Roveri, *Chem. Eur. J.* **2004**, *10*, 3043 – 3049.
[7] R. C. Sharma, Y. A. Chang, *Bull. Alloy Phase Diagrams* **1986**, *7*, 269 – 273.
[8] S. Del Buccia, J. C. Jumas, M. Maurin, *Acta Crystallogr. Sect. B* **1981**, *37*, 1903 – 1905.
[9] R. M. Hazen, L. W. Finger, *Am. Mineral.* **1978**, *63*, 289 – 292.
[10] S. Licht, G. Hodes, R. Tenne, J. Manassen, *Nature* **1987**, *326*, 863 – 864.
[11] M. Hangyo, K. Kisoda, T. Nishio, S. Nakashima, T. Terashima, N. Kojima, *Phys. Rev. B* **1994**, *50*, 12033 – 12043.
[12] Y. Shoji, T. Matsui, T. Nagasaki, M. Kurata, T. Inoue, *Int. J. Thermophys.* **2000**, *21*, 585 – 591.
[13] D. G. Mead, J. C. Irwin, *Solid State Commun.* **1976**, *20*, 885 – 887.
[14] A. J. Smith, P. E. Meek, Y. A. Liang, *J. Phys. C* **1977**, *10*, 1321 – 1333.
[15] A. Cingolani, M. Lugara, G. Scamarcio, *Nuovo Cimento Soc. Ital. Fis. D* **1988**, *10*, 519 – 528.
[16] H. R. Chandrasekhar, R. G. Humphreys, U. Zwick, M. Cardona, *Phys. Rev. B* **1977**, *15*, 2177 – 2183.
[17] P. M. Nikolic, L. Miljkovic, P. Mihajlovic, B. Lavrencic, *J. Phys. C* **1977**, *10*, L289 – L292.
[18] K. Trentelmann, *J. Raman Spectrosc.* **2009**, *40*, 585 – 589.
[19] Y. C. Zhang, Z. N. Du, S. Y. Li, M. Zhang, *Appl. Catal. B* **2010**, *95*, 153 – 159.
[20] H. Chang, E. In, K. J. Kong, J. O. Lee, Y. Choi, B. H. Ryu, *J. Phys. Chem. B* **2005**, *109*, 30 – 32.
[21] D. Porezag, T. Frauenheim, T. Kohler, G. Seifert, R. Kaschner, *Phys. Rev. B* **1995**, *51*, 12947 – 12957.
[22] G. Seifert, D. Porezag, T. Frauenheim, *Int. J. Quantum Chem.* **1996**, *58*, 185 – 192.